THE JOURNAL OF BIOLOGICAL CHEMISTRY
Vol. 254, No. 13, Issue of July 10, pp. 6068–6078, 1979
Printed in U.S.A.

Temperature and Compositional Dependence of the Structure of Hydrated Dimyristoyl Lecithin*

(Received for publication, December 5, 1978)

Martin J. Janiak,‡ Donald M. Small, and G. Graham Shipley§

From the Biophysics Division, Department of Medicine, Boston University School of Medicine, Boston, Massachusetts 02118

Differential scanning calorimetry and x-ray diffraction techniques have been used to investigate the structure and phase behavior of hydrated dimyristoyl lecithin (DML) in the hydration range 7.5 to 60 weight % water and the temperature range −10 to +60°C. Four different calorimetric transitions have been observed: T_1, a low enthalpy transition ($\Delta H \cong 1$ kcal/mol of DML) at 0°C between lamellar phases ($L \rightarrow L_{\beta'}$); T_2, the low enthalpy "pretransition" at water contents >20 weight % corresponding to the transition $L_{\beta'} \rightarrow P_{\beta'}$; T_3, the hydrocarbon chain order-disorder transition (ΔH = 6 to 7 kcal/mol of DML) representing the transition of the more ordered low temperature phases ($L_{\beta'}$, $P_{\beta'}$, or crystal C, depending on the water content) to the lamellar L_α phase; T_4, a transition occurring at 25–27°C at low water contents representing the transition from the lamellar $L_{\beta'}$ phase to a hydrated crystalline phase C. The structures of the $L_{\beta'}$, $P_{\beta'}$, C, and L_α phases have been examined as a function of temperature and water content. The $L_{\beta'}$ structure has a lamellar bilayer organization with the hydrocarbon chains fully extended and tilted with respect to the normal to the bilayer plane, but packed in a distorted quasihexagonal lattice. The $P_{\beta'}$ structure consists of lipid bilayer lamellae distorted by a periodic "ripple" in the plane of the lamellae; the hydrocarbon chains are tilted but appear to be packed in a regular hexagonal lattice. The diffraction pattern from the crystalline phase C indexes according to an orthorhombic cell with a = 53.8 Å, b = 9.33 Å, c = 8.82 Å. In the lamellar bilayer L_α structure, the hydrocarbon chains adopt a liquid-like conformation. Analysis of the hydration characteristics and bilayer parameters (lipid thickness, surface area/molecule) of synthetic lecithins permits an evaluation of the generalized hydration and structural behavior of this class of lipids.

Model systems consisting of either natural or synthetic lecithins have been a valuable tool in obtaining information on the structure of membranes and in understanding the interactions between phospholipids and other lipids and proteins. The phase behavior and structures associated with both isolated membrane phospholipids and their synthetic analogues have been investigated in detail since the development of the Davson-Danielli membrane model stressing the bimolecular leaflet arrangement (1). A wide range of physicochemical methods have shown that phospholipids undergo a temperature-dependent, reversible, order-disorder transition associated with melting of the hydrocarbon chain region of the lipid bilayers and this transition has been shown to be dependent on the fatty acid chain length and unsaturation, the degree of hydration, and the polar head group structure (for reviews, see Refs. 2–4).

While much effort has been devoted to the investigation of the structure of lecithin bilayers, some questions remain unanswered. For example, although the order-disorder transition of hydrated lecithins has been well documented (5, 6), the structural changes associated with other thermotropic and lyotropic transitions are not clearly defined. Thus, we have performed a comprehensive investigation of the phase behavior and structural features exhibited by dimyristoyl lecithin as a function of temperature (−10° to +60°C) and hydration (7.5 to 60 weight %) utilizing differential scanning calorimetry and x-ray diffraction methods.

MATERIALS AND METHODS

Dimyristoyl lecithin (DML) was synthesized in this laboratory using the method of Cubero Robles and Van Den Berg (7) and hydrated mixtures were prepared as previously described (8). DML[1] used in these studies contained only phosphatidylcholine as determined by thin layer chromatography and 99.9% of the total fatty acid components was myristic acid as determined by gas-liquid chromatography. Thin layer chromatography of hydrated samples after investigation by physical methods indicated that no chemical degradation of DML had occurred.

Samples taken for calorimetry (5 to 10 mg) were hermetically sealed in aluminum pans and placed in a Perkin-Elmer DSC-2 differential scanning calorimeter (Norwalk, Connecticut). Samples were studied at different heating rates between 0.31 and 10.0°C/min. Each sample was heated and cooled repeatedly between −10° and 60°C. Transition enthalpies were determined from the areas under the transition endotherm peak as measured by planimetry.

Nickel-filtered CuK$_\alpha$ x-radiation from an Elliott GX-6 rotating anode generator (Elliott Automation, Borehamwood, England) was collimated by double mirror optics (9) or toroidal optics (10). Samples were contained in thin-walled capillary tubes (internal diameter 0.7 mm) and x-ray diffraction patterns were recorded between −10° and 60°C utilizing a variable temperature specimen holder. Microdensitometry of x-ray diffraction photographs was carried out using a Joyce Loebl model III-CS microdensitometer. The data presented in Fig. 3 were obtained at Yale University (Department of Molecular Biophysics and Biochemistry) using line-focused Cu K$_\alpha$ x-radiation and a Tennelec (Oak Ridge, Tennessee) linear position sensitive detector.

The water content of the samples was determined gravimetrically at the time the mixtures were prepared for the x-ray diffraction and DSC experiments. Comparison was made between this determination

* This work was supported by United States Public Health Service Grants HL-18623, HL-13262, and HL-07291 from the National Institutes of Health. The costs of publication of this article were defrayed in part by the payment of page charges. This article must therefore be hereby marked "*advertisement*" in accordance with 18 U.S.C. Section 1734 solely to indicate this fact.

‡ Present address, Rigaku/U. S. A., Inc., 3 Electronics Ave., Danvers, MA 01923.

§ To whom correspondence should be addressed.

[1] The abbreviations used are: DML, dimyristoyl lecithin; DSC, differential scanning calorimetry; DLL, dilauroyl lecithin; DPL, dipalmitoyl lecithin; DSL, distearoyl lecithin; calorimetric transitions, T_1, low enthalpy transition; T_2, low enthalpy pretransition; T_3, the chain-melting order-disorder transition; T_4, transition from lamellar $L_{\beta'}$ phase to a hydrated crystalline phase C.

and measurement of water content after completion of x-ray diffraction and DSC studies to ensure that no water loss occurred during data collection.

RESULTS

Differential Scanning Calorimetry

Characteristic DSC thermograms of hydrated DML are shown in Fig. 1. At concentrations greater than 20 weight % water, two thermal transitions are observed: T_2, the low enthalpy pretransition and T_3, the high enthalpy chain-melting transition (Fig. 1*B*). These transitions are reversible and are observed on successive heating cycles. When the samples are cooled from 60°C, T_3 supercools and occurs ~2°C lower in temperature than observed on heating. T_2 exhibits supercooling and the transition temperature may be depressed by 8–12°C. Reducing the heating rate from 10 to 1.25°C/min also affects the transition temperatures. T_3 decreases in temperature by 1°C, but no change in the transition enthalpy is observed. T_2 appears to decrease in temperature on reduction of the heating rate; however, significant broadening of the transition occurs.

At concentrations <20% water, T_2 is no longer observed. A new transition, T_1, occurring near 0°C, is now observed prior to T_3, which is now broadened and occurs at higher temperature. These transitions are reversible and are observed on successive heating cycles. The transition, T_1, has not been observed previously.

At lower hydration states (<15% water), T_3 is further broadened and shifted to higher temperature. This transition is now accompanied by an overlapping transition, T_4, (Fig. 1*A*), again a transition previously unobserved. Unlike the other thermal transitions, T_4 is not observed on subsequent heating of the sample and only a single transition is observed at a temperature intermediate between T_4 and T_3. However, if the sample is held at −20°C for several hours and then heated, the transitions T_4 and T_3 reappear at the original temperatures.

A summary of the temperature dependence of these transitions observed by DSC as a function of hydration is shown in Fig. 2. Both the onset temperature of the transition and the endotherm maximum are plotted where possible. Four distinct transitions are observed. (i) T_1 (◇), a broad low enthalpy transition ($\Delta H \cong 1$ kcal/mol of DML) occurs near 0°C between concentrations of 10 and 25% water. (ii) T_2 (□), the so-called "pretransition," occurs at all water contents >20%. The onset temperature remains at 11°C, while the endotherm maximum increases in temperature from 13°C at 30% water to 20°C at 21% water. In addition, there is an associated increase in the transition enthalpy with a decrease in water content. At concentrations >30% water, the transition enthalpy is 1.0 kcal/mol, in agreement with previously reported values (8, 11). At 22.8% water, the enthalpy is larger, 1.8 kcal/mol. (iii) T_3 (○), the "chain-melting," order-disorder transition, occurs at all water concentrations studied. At concentrations <30% water, the transition begins to broaden and the transition temperature increases. Associated with an increase in the transition temperature is an increase in the enthalpy: ΔH(@ 21% water) = 6.3 kcal/mol, ΔH(@ 17% water) = 6.7 kcal/mol. (iv) T_4 (△), this transition occurs in a narrow compositional range between 9 and 14% water, at temperatures of 25–27°C. Since this transition overlaps with T_3, an accurate measurement of the transition enthalpy could not be established.

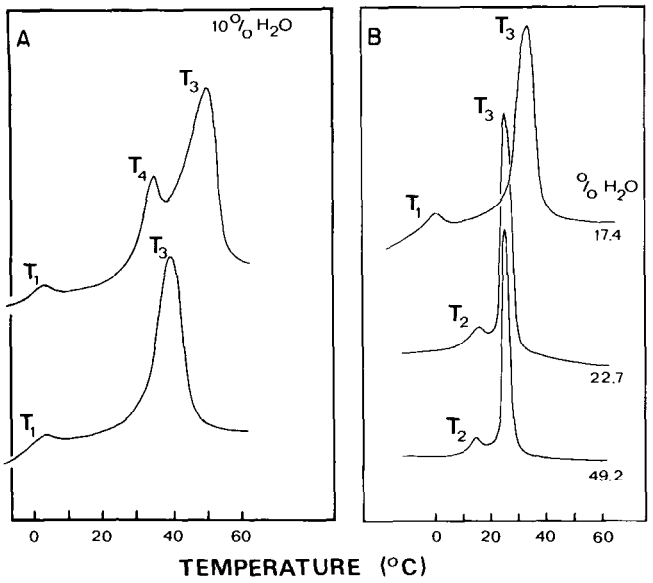

FIG. 1. DSC thermograms of hydrated DML representative of the compositional range (*A*) 9 to 14% water (*upper curve*, first heating; *lower curve*, second heating) and (*B*) >15% water. The heating rate was 5°C/min.

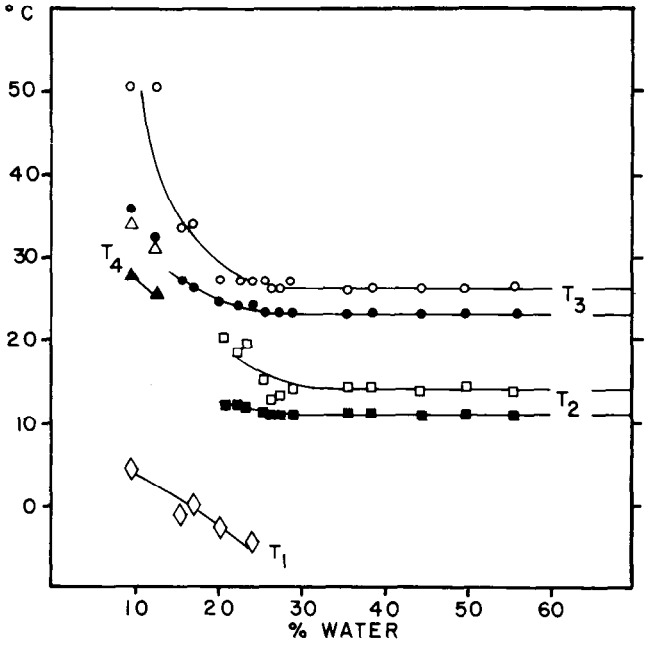

FIG. 2. Thermal transitions T_1 (◇), T_2 (□), T_3 (○), and T_4 (△), observed by DSC for hydrated DML as a function of composition. Transitions plotted for data obtained by heating sample at 5°C/min. *Solid symbols*, transition onset temperature; *open symbols*, temperature of endotherm maxima.

X-ray Diffraction

Twenty-one Per Cent Water (Characterization of T_2 and T_3)

Changes in the characteristic x-ray diffraction patterns associated with the thermal transitions T_2 and T_3 have been obtained at water concentrations >20%. These transitions have been previously characterized (8). At temperatures $<T_2$, several sharp low angle reflections in the ratio 1:1/2:1/3:1/4, etc., characteristic of a one-dimensional lamellar lattice are observed. At high angles, a sharp diffraction maximum centered at $s = (4.2\ \text{Å})^{-1}$ together with a broader band at higher scattering angles is observed. At temperatures intermediate between T_2 and T_3, these lamellar reflections are present but accompanied by many additional reflections arising from a two-dimensional oblique lattice (see Fig. 3). At temperatures above T_3, only lamellar reflections are observed together with

a diffuse diffraction band centered at (4.5 Å)$^{-1}$ in the high angle region.

Sixteen Per Cent Water (Characterization of the Mixtures Containing 15 to 20% Water)

X-ray diffraction data were collected between 10° and 60°C in this region. DSC data indicated that T_2 is no longer present and only T_3 is observed. At all temperatures (Fig. 4), only reflections arising from a one-dimensional lattice, L, were observed. In this water concentration range, T_3 is significantly broadened. As shown in Fig. 4*B*, at temperatures near the endotherm maximum of T_3, two sets of lamellar reflections are present: the lower temperature phase $<T_3$ (Fig. 4*A*) and that from the phase present at $>T_3$ (Fig. 4*C*). The higher temperature phase $>T_3$ gives the same diffraction pattern as that obtained at higher water concentrations for the structure L_α.

The diffraction pattern shown in Fig. 4*D* was obtained under the same conditions used to observe the two-dimensional lattice. Nonlamellar reflections could not be detected in any mixture in this compositional range, in agreement with the absence of the pretransition T_2 by DSC. In the high angle region of the diffraction pattern, a sharp reflection at s_1 = (4.25 Å)$^{-1}$ well separated from a broad band at s_2 = (4.16 Å)$^{-1}$ is observed. This corresponds to a deformed hexagonal lattice of tilted chains, each rod separated by four rods at 4.87 Å and two rods by 4.77 Å. Thus, in this compositional range, the structure corresponds to $L_{\beta'}$ below T_3 and at T_3, the structure transforms to L_α (6).

Ten Per Cent Water (Characterization of T_1 and T_4)

At temperatures $<T_1$, we could not obtain sufficient x-ray diffraction data to define the structure completely. However, as shown in Fig. 5, only reflections arising from a one-dimensional lattice were observed and the Bragg spacings were very similar to those obtained above the T_1 transition. At high angles, a sharp maximum at (4.2 Å)$^{-1}$ together with a broad band at (3.98 Å)$^{-1}$ is observed. At temperatures intermediate between T_1 and T_4, the diffraction pattern shown in Fig. 6*a* is

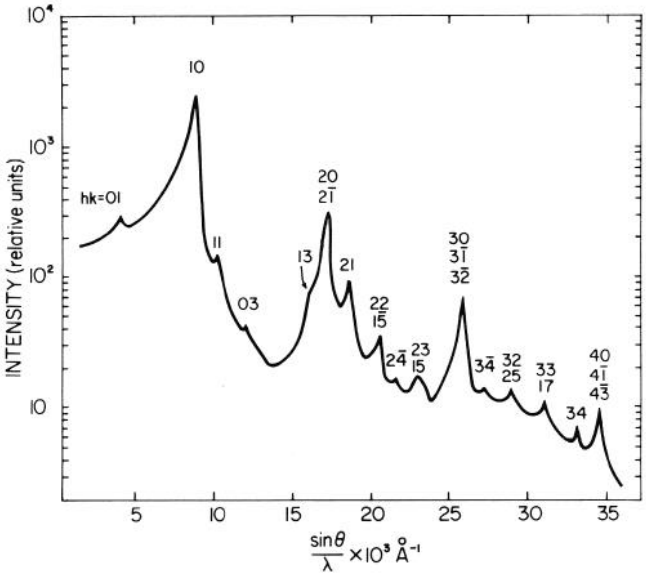

FIG. 3. X-ray diffraction pattern of hydrated DML containing 22.3% water at 20°C obtained using a linear position-sensitive detector. At temperatures $<T_2$ and $>T_3$ only reflections with Miller indices $h0$ are observed.

obtained. At low angles, only lamellar reflections are observed. At high angles, a sharp maximum at (4.25 Å)$^{-1}$ and, in some cases, an additional maximum at (4.22 Å)$^{-1}$, is observed together with a broader band at (4.16 Å)$^{-1}$. These reflections probably arise from large lamellar domains which possess slightly different chain packing characteristics. For example, this diffraction pattern would result if one region of the lipid lamellae contained tilted chains whose hexagonal lattice was deformed more than the other, but the tilt of the chains remained approximately the same. Since the tilt of the chains is the same for each region of domain, the lamellar repeat distance would be identical and only a single set of low angle reflections would be observed. The observed high angle reflections would be produced from two deformed lattices of

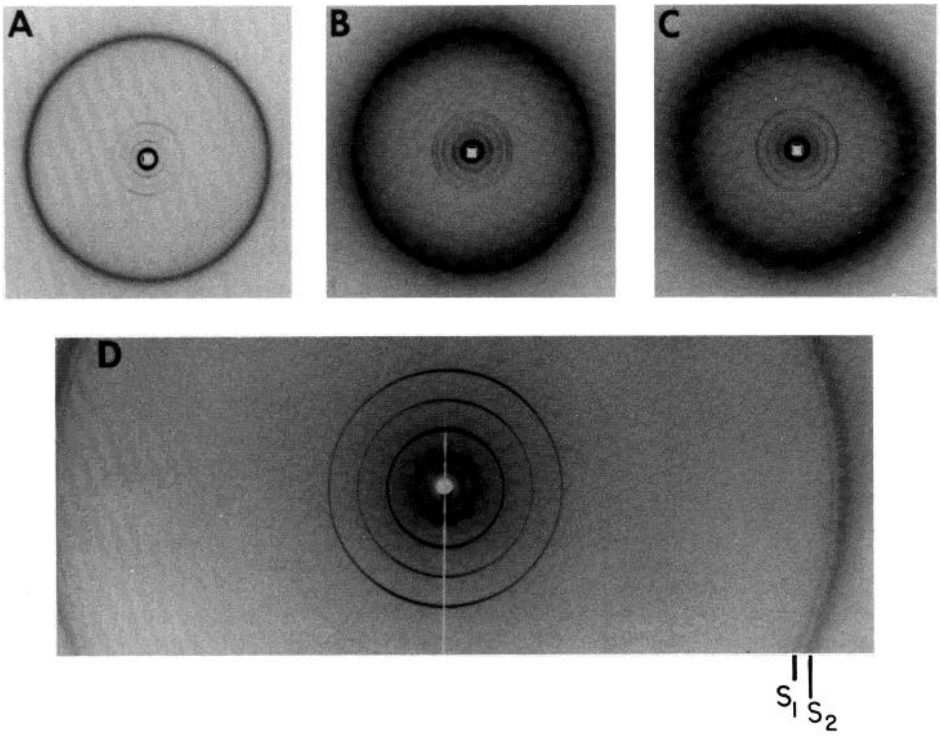

FIG. 4. X-ray diffraction patterns for hydrated DML containing 16% water at temperatures $<T_3$: *A*, 10°C; *D*, 20°C; and *B*, 37°C. At temperatures $>T_3$: *C*, 60°C.

tilted chains: 1) each rod surrounded by four rods at 4.84 Å and two at 4.77 Å, and 2) each rod surrounded by four rods at 4.84 Å and two at 4.78 Å, *i.e.* a structure closely related to the $L_{\beta'}$ structure observed at higher water contents (see above). The similarity in the interlamellar repeat distance below the T_1 transition suggests that the low temperature structure is not drastically different from $L_{\beta'}$ and may arise from subtle alterations in the hydrocarbon chain packing. However, sufficient data have not been obtained to classify this structure further.

At temperatures intermediate between T_4 and T_3, a powder diffraction pattern from a crystalline phase, C, is observed

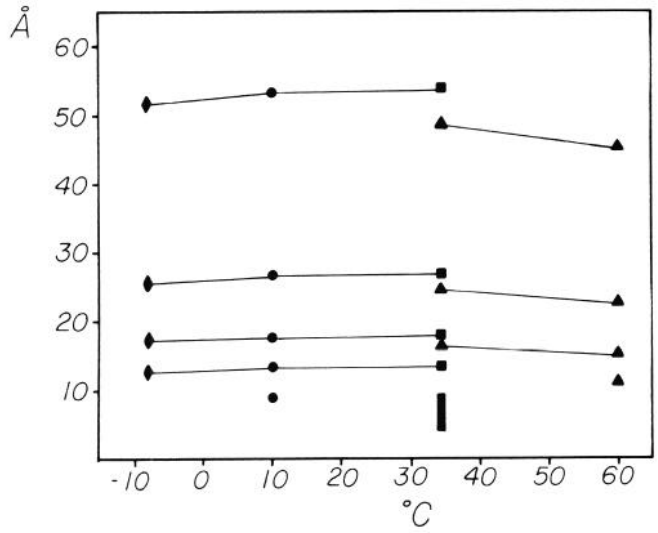

FIG. 5. Temperature dependence of the low angle x-ray diffraction reflections from hydrated DML containing 10% water. ◆, $<T_1$; ●, T_1 to T_4; ■, T_4 to T_3; ▲, $>T_3$.

(Fig. 6*b*). At the temperature studied, 34°C, the higher temperature $L_{\beta'}$ phase was also observed coexisting with this phase (see Fig. 6*a*). At temperatures $>T_3$, the structure transforms to L_α as previously described.

From the identification of the x-ray diffraction patterns associated with specific temperature and composition ranges, a more detailed analysis of the specific structures can now be described.

(a) The Crystal Phase—The observed reflections for this crystal phase were indexed according to an orthorhombic cell, $a = 53.8$ Å, $b = 9.33$ Å, $c = 8.82$ Å (Table I). Since two phases were present at this temperature (see above), the distribution of water between the phases is not known. In addition, neither the partial specific volume, $\bar{v}_l$, of the crystal nor the number of molecules per unit cell, Z, can be determined unequivocally. The compositional data indicates the sample contains ~4 water molecules/molecule of DML. From the cell volume, only 4 DML molecules can occupy the cell. To estimate the number of water molecules per cell, $\bar{v}_l$ was calculated assuming 4 DML and 0 to 16 water molecules per unit cell. Previous estimates from powder x-ray data obtained from a crystal phase of DML assumed to be the monohydrate gave a value of $\bar{v} = 0.95$ (6). The $\bar{v}$ for fully hydrated DML varies from 0.935 to 0.950 depending on the temperature between 0 and 20°C (12). These values probably represent limiting values of $\bar{v}_l$ for DML. Thus, it is reasonable to conclude that the unit cell contains between 4 and 8 water molecules.

The cell parameters obtained here are different than those previously reported for DML containing lesser amounts of water (13); these were $a = 47.6$ Å, $b = 8.65$ Å, $c = 10.7$ Å. Although the cell parameters are different, the cell volumes are very similar.

(b) The $L_{\beta'}$ Phase—The low angle x-ray diffraction data show that a one-dimensional lattice, L, exists at all water concentrations at some temperature interval below T_3, the

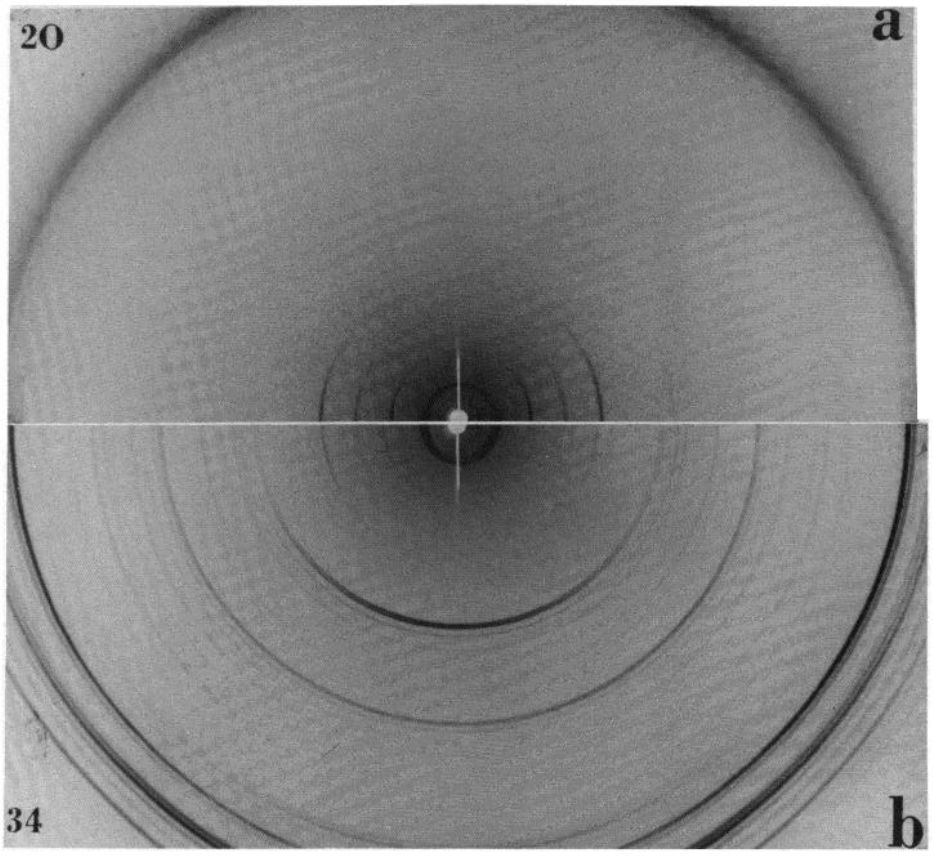

FIG. 6. X-ray diffraction pattern obtained for hydrated DML containing 10% water. At temperatures $<T_4$: *a*, 20°C. At temperatures intermediate between T_4 and T_3: *b*, 34°C.

TABLE I

Comparison of calculated and observed Bragg spacings for the crystalline phase C

For a mixture containing 10 weight % water. Cell parameters: a = 53.8 Å, b = 9.33 Å, c = 8.82 Å.

h	k	l	S^{-1} observed	S^{-1} calculated
1	0	0	53.85	53.85
2	0	0	26.94	26.93
3	0	0	17.96	17.95
4	0	0	13.63	13.64
0	1	0	9.33	9.33
1	0	0	9.18	9.19
0	0	1	8.82	8.82
3	1	0	8.28	8.28
4	1	0	7.36	7.37
5	1	0	7.08	7.06
1	1	1	6.35	6.36
2	1	1	6.23	6.21
3	1	1	6.01	6.03
4	1	1	5.79	5.78
5	1	1	5.51	5.51
8	0	1	5.36	5.35
6	1	1	5.23	5.22
9	0	1	4.94	4.95
2	0	2	4.35	4.35
2	0	3	4.29	4.28
2	0	4	4.20	4.19

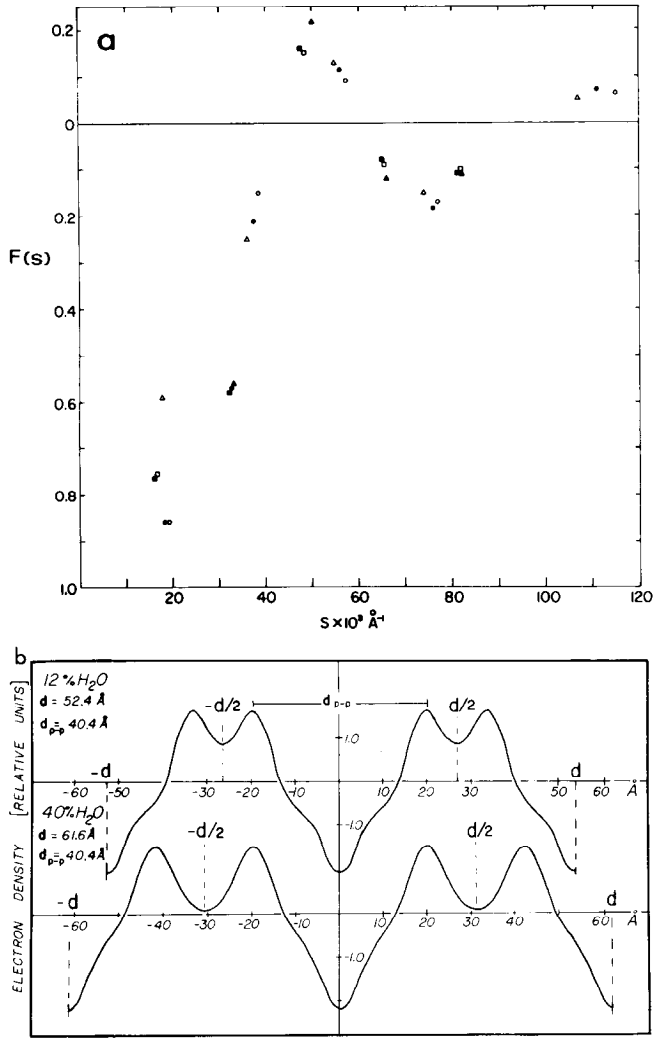

FIG. 7. The $L_{\beta'}$ phase. *a*, relative amplitudes with assigned phases for mixtures containing (○) 12.0%, (●) 16.7%, (△) 21.7%, (▲) 28.2%, (□) 40.5%, and (■) 55.1% water. *b*, representative electron density profiles; $-d/2$ to $d/2$ represents one unit cell; $d_{p\text{-}p}$ represents the bilayer thickness.

chain-melting transition. The x-ray diffraction data obtained at 10°C is analyzed to determine the structural features of this one-dimensional lattice and to investigate further the conformation of the hydrocarbon chains. The measured intensities for a series of mixtures containing between 12 and 55% water vary with changes in hydration. For example, at lower water contents the fifth order is not measurable, but increases in intensity at higher water contents. Although this one-dimensional unit cell repeat varies over the range of hydrations, the structural changes in the bilayer itself may be assumed to be small and there is an average structure whose transform is sampled with varying hydration (14). While the transform could not be reconstructed on an absolute scale, normalization of the data enables the transform to be determined on a relative scale. The high angle data indicates that the hydrocarbon chains are in a crystalline-like state and display only minor variations in packing as a function of composition. Thus, it can be assumed that the total diffracted intensity at high angle is invariant as a function of hydration and the low angle data can be normalized by I $(h)/I$ (high angle). The observed intensities for all mixtures were corrected for Lorentzian polarization and normalized. $I^{1/2}$ was plotted *versus* s ($s = 2\sin\theta/\lambda$) over the range of s values sampled (see Fig. 7*a*). From the intensity distribution, the values of s at which $F(s) = 0$ (the nodes) can be approximately determined and a set of phases (0 or π for this centrosymmetric structure) can be determined for the structure amplitudes obtained at each hydration value. The node determined at $s = 0.098$ Å^{-1} correlates well with the observed absence of the fifth order at low water contents.

Using these phased values of $F(s)$, the Fourier transform is calculated and the low resolution profile is obtained (Fig. 7*b*). The features of the profile are consistent with those previously obtained for other hydrated phospholipids exhibiting this structure (6, 13). The maximum in electron density corresponds to the polar head group of DML, the peak to peak separation approximating the bilayer thickness, and the central trough is typical of crystalline hydrocarbon chains whose terminal methyl groups are localized in the center of the bilayer. All the profiles obtained are nearly identical with only the region of the water layer varying in dimension. The peak to peak separations ($d_{p\text{-}p}$) are invariant at ~40 Å.

These data are now compared with the calculated structural parameters determined from the interlamellar repeat, d. The hydration dependence of the interlamellar repeat is shown in Fig. 8*a*; d increases from 53.6 Å at ~18% water to a limiting maximum value of 61.7 Å at 29% water. The calculated lipid thickness, d_l, (Fig. 8*b*), decreases with increasing water content from 47.1 Å at 10% water to 42.4 Å at ~25% water, remaining constant thereafter. Only small differences occur between d_l and $d_{p\text{-}p}$ (~2 Å) at water contents >20%. At the resolution of the electron density calculations (~6 Å), the value of $d_{p\text{-}p}$ would be expected to be less than the actual bilayer thickness and is consistent with the observed differences.[2] On decreasing the water content to less than 20%, the difference between d_l and $d_{p\text{-}p}$ increases to ~5 Å at 12% water. This difference may be due to the low resolution of the electron density profiles. However, it is noteworthy that 20% water corresponds to the amount of water tightly bound to the polar head group. It is possible that the partial specific volume of the lipid may vary at low water contents and account for these differences.

Both values, d_l and $d_{p\text{-}p}$, are consistent with the hydrocarbon chains of DML being tilted with respect to the plane of the lamellae in agreement with the high angle x-ray data. If the hydrocarbon chains of DML are rigid and fully extended, one would predict the bilayer thickness to be 51.6 Å based on

[2] G. G. Shipley, unpublished observations.

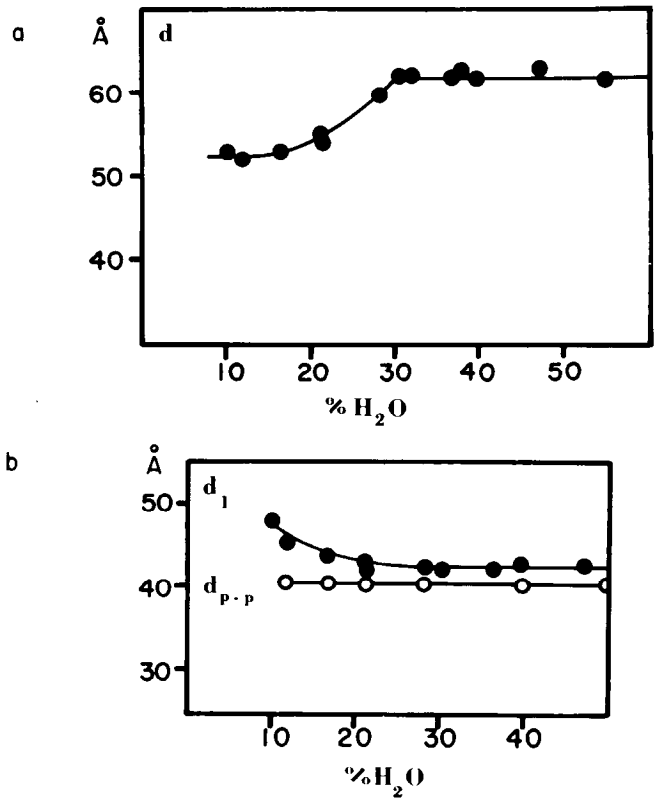

FIG. 8. *a*, bilayer repeat distance, *d*, for hydrated DML as a function of composition at 10°C. *b*, calculated bilayer thickness, d_l (●), compared with $d_{p\text{-}p}$ (○) determined from electron density profiles (see Fig. 7*b*, for example).

molecular model building. Both d_l and $d_{p\text{-}p}$ are considerably less than this value. At 10°C, the calculated average angle of tilt with respect to the normal to the plane of the lamellae is ~35° for water contents >20%.

(c) The $P_{\beta'}$ Phase—As stated above, T_2 is associated with the formation of $P_{\beta'}$ and the two-dimensional lattice probably arises from periodic distortions of the lamellae. We have previously described the compositional dependence of the cell parameters *a* and *b* at 20°C (8). The *a* parameter increases in similar fashion to the interlamellar repeat of the $L_{\beta'}$ phase increasing from 57 Å at 21% water to a maximum value of 64.9 Å at 29%, while *b* decreases sharply from 156 Å at 21% to a minimum value of 120 Å at 29% water. These variations are accompanied by marked differences in the sampled diffraction at the upper and lower compositional limit of the structure as illustrated in Fig. 9.

The diffraction data are further analyzed in an attempt to understand the physical basis of the compositional dependence of this structure. The approach taken is to construct a set of model structures consistent with the physical and chemical nature of the system and determine the best fit of the calculated values with the observed data. The choice of models is based on previous structural studies on phospholipid systems. Under certain temperature and hydration conditions, egg lecithin and phosphatidic acid are thought to form "peristaltic" structures (15). In this structure, some regions contain disordered hydrocarbon chains and others ordered as shown in Fig. 10*A*. Although this hydrocarbon chain conformation is not consistent with the observed high angle x-ray diffraction data, this model is considered as a possible structure. Diffraction data similar to that described here has been observed for dilauroyl lecithin (DLL) at −7°C and for DML at 19°C (6). The structure associated with this diffraction pattern was interpreted as stacked lamellae distorted by a periodic "ripple" in the plane of the lamellae (Fig. 10*B*). Other structures such as a "sawtooth" model are also considered (Fig. 10*C*). However, this model is not consistent with the chemical nature of the DML molecule; such a structure would expose significant hydrophobic regions of the molecule to the polar water layer. Preliminary calculations for this model were not consistent with the observed x-ray diffraction data, in agreement with other model analyses (13), and this model will not be considered in further detail.

The basis for calculating structure factors is as follows. Strip models to depict electron density distributions across phospholipid bilayers indicate the resulting diffraction pattern is due to the interference of a positive double slit (headgroup) with a negative slit (terminal methyl group) (16). Using this premise, a simple two-dimensional model consisting of a set of points positioned in the unit cell corresponding to the polar groups, $f(1)$, and terminal methyl groups, $f(2)$, was constructed for the peristaltic model (Fig. 10*E*) and ripple model (Fig. 10*D*). Thus, the model is simply a set of six functions, whose amplitude is $\pm f(1)$ and $\pm f(2)$, translated through the unit cell by some function.

In order to calculate structure factors (F_c) for the peristaltic and ripple models for the corresponding region of reciprocal space sampled in the observed diffraction pattern, the only input parameters required were the cell parameters *a*, *b*, and γ; the Bragg value of the 10 reflection; the calculated lipid thickness, d_l; the ripple or peristaltic oscillation amplitude, *Q*; and the amplitude of the functions, $f(1)$ and $f(2)$, describing

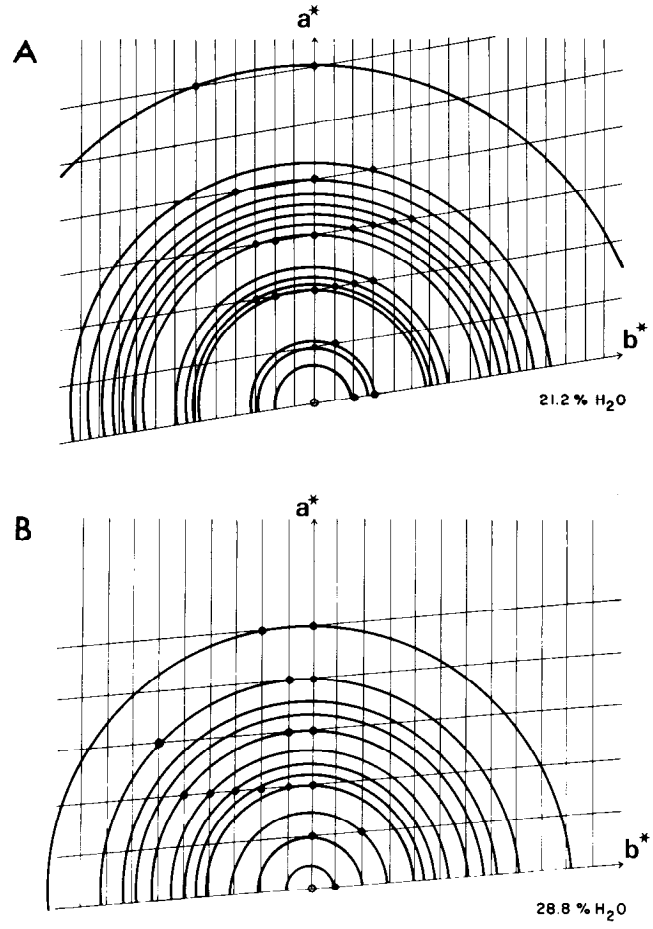

FIG. 9. The reciprocal lattice of the two-dimensional $P_{\beta'}$ structure at its lower (*A*) and upper (*B*) compositional limits. The radii of the circles represent the reciprocal spacings of the observed reflections and the points represent their indexing on the two lattices. a* and b* are the reciprocal cell axes.

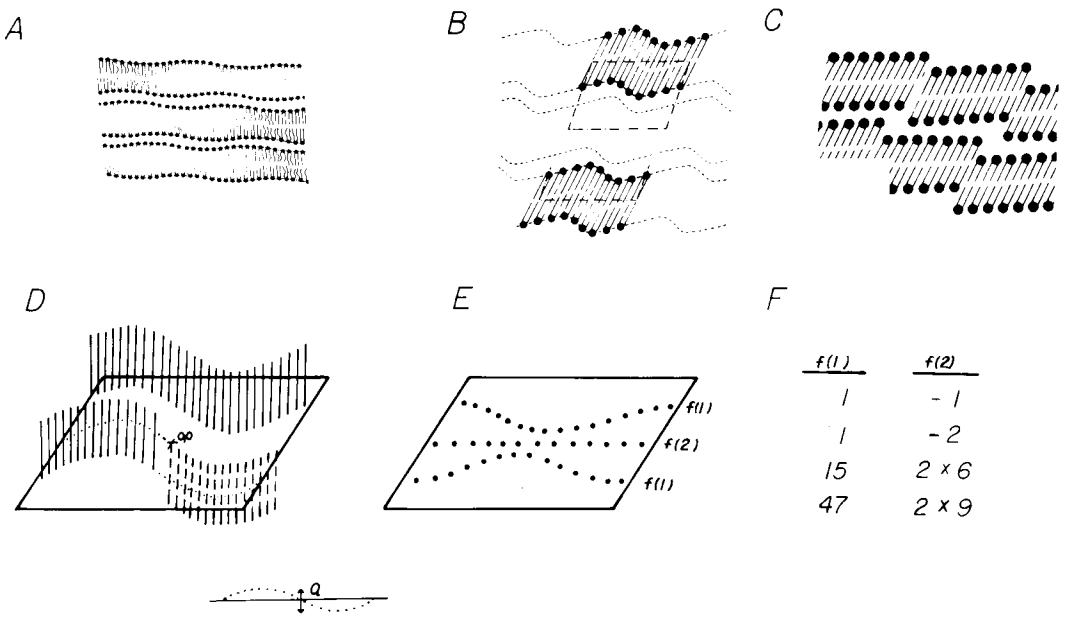

FIG. 10. Models for the $P_{\beta'}$ structure. *A*, a peristaltic structure (see Ref. 15); *B*, a rippled structure (see Refs. 8 and 13); *C*, a sawtooth model (see Ref. 6); *D*, for the ripple model used in the calculations, ○,○ represents the origin; *E*, the peristaltic model used in the calculations; *F*, the values of the amplitudes of the δ functions used in the calculation of the Fourier transform. $f(1)$ represents the polar region and $f(2)$ the terminal methyl region of the DML molecule.

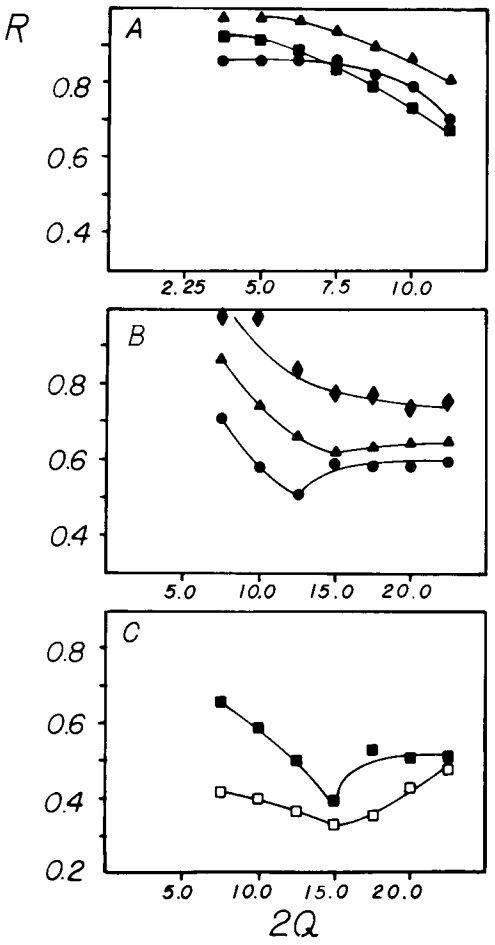

FIG. 11. Calculated R values as a function of $2Q$ for (*A*) the peristaltic model and (*B* and *C*) the ripple model. ▲, $f(1) = 47$, $f(2) = 18$; ■, $f(1) = 1.0$, $f(2) = 2.0$; ●, $f(1) = 1.0$, $f(2) = -1.0$; ◆, $f(1) = 15.0$, $f(2) = 12.0$. *Closed symbols,* data at 30% water; *open symbols* in *C*, data at 20% water.

TABLE II

Calculated and observed data at the lower compositional limit for the $P_{\beta'}$ phase

For a mixture containing 21% water. Cell parameters: $a = 55.9$ Å, $b = 160.9$ Å, $\gamma = 99°$. Temperature factor, $B = 60$.

h	k	S^{-1} calculated	S^{-1} observed	F_c	$\lvert F_o \rvert$
		Å			
0	2	80.3	79.1	−13.7	19.0
1	0	55.4	55.3	−232.7	317.2
1	1	55.1		−77.1	
1	1	49.9	49.9	+82.4	85.0
1	2	49.3		−11.6	
2	0	27.7	27.6	−31.1	107.9
2	2	27.5		−15.4	
2	1	26.6	26.5	+49.7	75.1
2	3	26.3		−19.9	
2	2	24.9	24.6	−15.4	36.3
2	4	24.6		−21.6	
2	3	23.2	22.8	+24.7	27.5
3	2	18.6		−87.4	
3	0	18.4	18.4	+1.6	84.2
3	3	18.3		−29.9	
3	2	17.4	17.3	−87.4	41.2
3	5	17.2		+18.4	
3	3	16.5	16.5	+35.8	25.4
3	4	15.9	15.8	+11.0	21.5
3	5	15.0	15.0	−16.1	26.4
4	0	13.8	13.8	+102.4	98.3
4	3	13.9		+12.4	
4	3	12.9	12.9	−11.9	
5	0	11.1	11.1	−29.8	42.0
5	5	11.0		+6.8	39.5
6	0	9.2	9.2		

TABLE III

Calculated and observed data at the upper compositional limit for the $P_{\beta'}$ phase

For a mixture containing 30% water. Cell parameters: a = 59.6 Å, b = 118.0 Å, γ = 95°. Temperature factor, B = 60.

h	k	S^{-1} calculated	S^{-1} observed	F_c	$\|F_o\|$
		Å			
0	1	118.2	118.2	−1.7	38.4
1	0	60.9	60.7	−191.2	210.6
0	2	59.1		+27.9	
1	2	41.0	39.7	−3.4	36.8
0	3	38.4		+2.9	
2	0	30.5	30.4	−98.2	148.3
2	1	30.3		−53.1	
2	2	27.9	28.0	+5.1	72.0
1	4	27.3		−6.5	
2	3	25.1	25.0	−23.2	47.1
2	4	22.6	22.2	−29.4	35.7
1	5	21.9		+9.8	
3	0	20.3	20.5	+5.6	64.4
3	1	20.3		−51.2	
3	2	18.8	18.7	−108.0	62.8
3	3	18.6		−35.7	
3	4	16.6	16.6	+15.6	40.6
3	5	16.0		+16.0	
4	0	15.2	15.2	+57.5	44.4
4	1	14.9		+1.1	
4	4	13.2	13.4	−18.5	43.8
4	5	13.3		−34.8	
5	0	12.2	12.0	+77.4	55.2
5	1	12.2		−26.6	

the polar head and terminal methyl regions. For each set of cell parameters, several choices of $f(1)$ and $f(2)$ were used in the calculation; these values varied from equal magnitudes but opposite sign to values proportional to the electron content of the polar and terminal methyl region (see Fig. 10*F*). For each choice of $f(1)$ and $f(2)$, Q was varied from 2.5 Å to 11.25 Å for the ripple model, from 1.12 Å to 5.63 Å for the peristaltic model, and the calculated structure factor, F_c, was determined. By comparison with the observed structure factors, F_o, an R value was calculated according to

$$R = \frac{\sum \left| |F_o| - |F_c| \right|}{\sum |F_c|}$$

For this analysis, two data sets are compared: that at the lower compositional limit for $P_{\beta'}$, 21% water, and the upper compositional limit, 30% water. These results are summarized in Fig. 11 where R is plotted as a function of $2Q$. $2Q$ more precisely represents the physical nature of the undulation and is the peak to trough distance of the undulation. For example, for the ripple model, $2Q$ = 5 Å indicates a shallow undulation and $2Q$ = 22.5 Å is a very drastic distortion. Similarly, for the peristaltic model, $2Q$ = 11.25 Å allows for no hydrocarbon region in certain portions of the bilayer and hence is not physically realistic. For the peristaltic model (Fig. 11*A*), no value of $2Q$ and choice of $f(1)$ and $f(2)$ gave an R value of less than 0.6. For the ripple model (Fig. 11*B* and *C*), a lower R value was obtained for any choice of $f(1)$ and $f(2)$ compared to the peristaltic model. In addition, a defined minimum was observed for the ripple model. The lowest value of R for the ripple model was calculated for a value of $2Q$ = 15 Å, $f(1)$ = 1.0, $f(2)$ = −2.0 for both data sets, and R = 0.39 at 30% water, and R = 0.33 at 21% water. A constant ripple amplitude is consistent with the calculated number of molecules per unit cell decreasing from ~38 at 21% water to ~30 at 30% water. Using the calculated and observed structure factors, an isotropic temperature factor correction was determined. The final R obtained was 0.37 at 30% water and 0.26 at 21% water. The calculated and observed structure factor data is summarized in Tables II and III.

(d) The L_α Phase—As noted earlier, the L_α phase has been extensively studied but a complete hydration dependence determination has not been carried out for DML. In the previous sections, we have described the presence of this structure at temperatures $>T_3$, the chain-melting transition, over all compositions studied.

At 37°C, the interlamellar repeat distance, d, increases with increasing hydration in similar fashion to egg lecithin from ~48 Å, between 10 and 21% water, to its limiting value of 62.2 Å at 40% water, remaining constant thereafter (Fig. 12*A*). It is interesting to note the invariance in d between 10 and 21% water. Similar behavior was observed for egg lecithin where d was invariant between 5 and 15% water. For DML, d begins to increase at 21% which corresponds to the point at which free water (*i.e.* that which is not tightly bound to the polar head group) is present. This appears to be the same point at which the bilayer thickness, d_l, begins to deviate from its minimum value, 35.5 Å (Fig. 12*B*). Since the surface area, S_l, is inversely proportional to d_l, it increases and reaches a limiting value of 62.2 Å (Fig. 12*C*). Thus, it appears that perturbations to the structure are complete at the point at which free interstitial water exists between the bilayers.

DISCUSSION

The Phase Behavior of DML-Water—From the calorimetric and x-ray diffraction data, the temperature-composi-

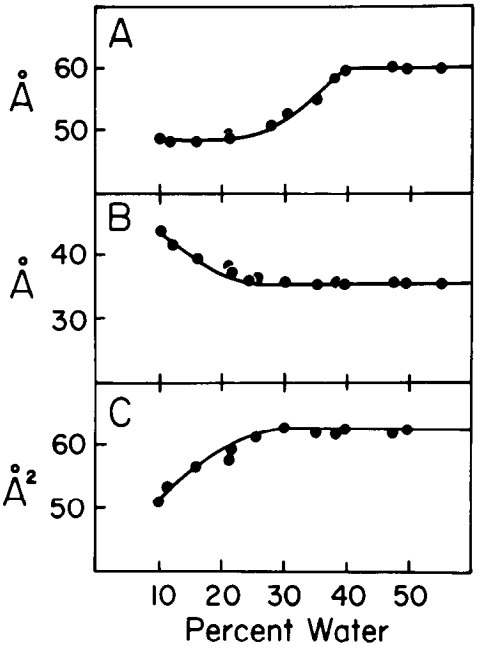

FIG. 12. Compositional dependence for DML in the L_α phase at 37°C of: (*A*), bilayer repeat distance, d; (*B*), lipid thickness, d_l; and (*C*), surface area/DML molecule.

tion phase diagram of hydrated DML for water contents between 5 and 60 weight % was constructed and is presented in Fig. 13. At low temperature (≦0°C) and water content (~5 to 20%), a lamellar structure, L, exists. The similarity in the diffraction pattern and lamellar repeat distance to that found at higher temperature suggests that no major structural alteration occurs at the T_1 transition. T_1 may arise from either packing alterations in the hydrocarbon region (lattice rearrangement) or intermolecular rearrangement of the highly structured interstitial water with the polar head group of the phospholipid.

In the entire compositional range described, the structure $L_{\beta'}$ exists at temperatures $<T_2$ and at lower water contents $<T_4$ or T_3. In this one-dimensional structure, the hydrocarbon chains are fully extended and tilted with respect to the plane of the bilayer, but packed in a distorted quasihexagonal lattice. Increasing the temperature results in packing alterations such that the hexagonal lattice becomes less distorted. The average angle of tilt of the hydrocarbon chains decreases with increasing temperature. This is in contrast to the tilt angle as a function of hydration where low resolution electron density profiles indicate little or no change. The swelling limit of DML occurs at ~30 weight % water for this structure.

The pretransition, T_2, is associated with a structural transformation from a one-dimensional (lamellar) to a two-dimensional structure, $P_{\beta'}$, consisting of lipid lamellae distorted by a periodic ripple in the plane of the lamellae. This two-dimensional structure does not vary significantly with temperature between T_2 and T_3, but its unit cell parameters a and b do exhibit a compositional dependence. The cell parameter a increases with increasing water content proportional to the amount of water intercalated between the lipid bilayers in the swelling lecithin, its maximum value occurring at the swelling limit of the lecithin (~30% water). Associated with an increase in a, is a decrease in the b cell parameter, measuring the period of the ripple. At the swelling limit of the lecithin, its value reaches a minimum. The model calculations suggest that the depth of the ripple is ~15 Å and that this parameter does not vary significantly with hydration. At T_2, the angle of tilt of the hydrocarbon chains reaches a minimum value remaining invariant thereafter and the cross-sectional chain packing is now a regular hexagonal array (8). At water contents <20%, T_2 is no longer present and the structure $L_{\beta'}$ predominates. The fact that in this hydration region (<20% water, 11°C to T_3) the hydrocarbon chains remain in a distorted quasihexagonal lattice suggests that the formation of a regular hexagonal lattice may accompany the formation of the $P_{\beta'}$ phase.

In a narrow range of composition (9 to 14% water) and temperature (27–35°C), a crystalline phase, C, is present. This structure appears to be a hydrated DML crystalline phase and may coexist with other phases. At the chain-melting transition, T_3, all of the low temperature structures convert to the one-dimensional lamellar structure, the phase L_α, at all water contents studied. In this structure, the hydrocarbon chains assume a liquid-like conformation. At lower water contents, a well defined two-phase region exists containing the phase L_α and one of the lower temperature phases C, $L_{\beta'}$, or $P_{\beta'}$, depending on the degree of hydration. The swelling limit of DML occurs at 40% water for the L_α phase, after which water exists as a separate phase.

Generalized Phase Behavior of Hydrated Synthetic Lecithins—From the similarities in structure and phase behavior, we propose a generalized phase behavior for the synthetic lecithins. First, consider the structural changes that occur at the pretransition; similar structural changes were observed for dilauroyl lecithin (6) and dipalmitoyl lecithin (8). Thus, it is reasonable to suggest that the structural transformation from $L_{\beta'}$ to $P_{\beta'}$ is common to all the synthetic lecithins exhibiting a thermal pretransition. Supporting evidence is found in freeze-fracture electron microscopy studies on synthetic lecithins. Rippled structures have been observed when synthetic lecithins are quenched from a temperature below the chain-melting transition, but not for heterogeneous acyl chain leci-

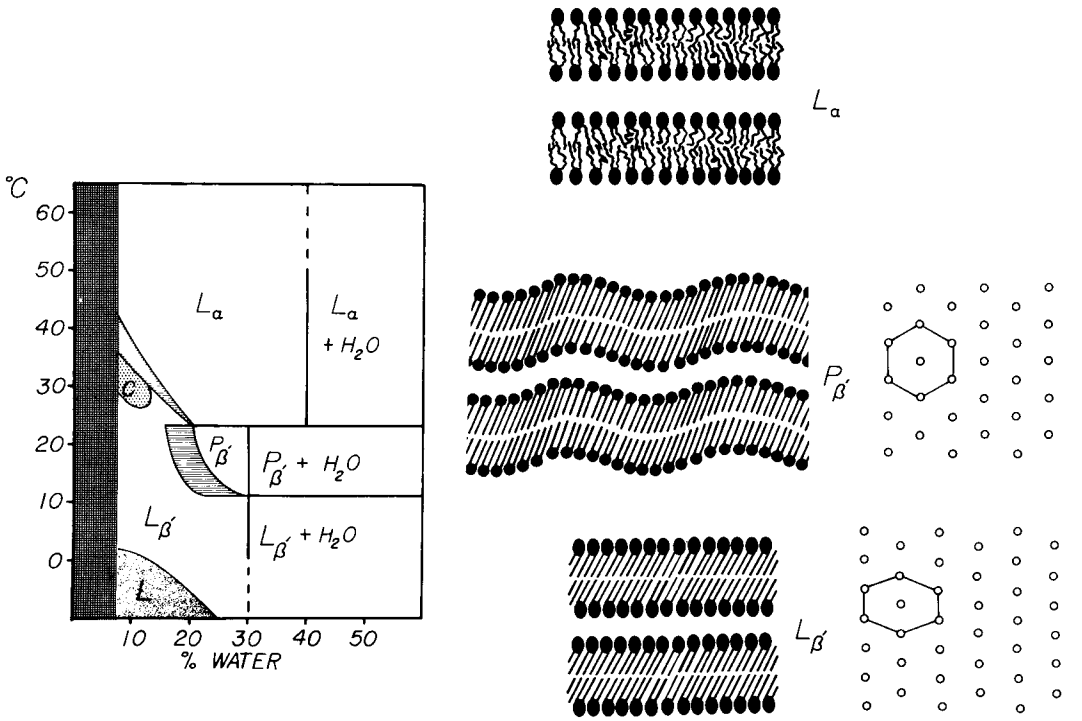

FIG. 13. Temperature-composition phase diagram of hydrated DML, together with representations of structures $L_{\beta'}$, $P_{\beta'}$, and L_α. The hydrocarbon chain packing is a hexagonal array for the $P_{\beta'}$ phase and a "distorted" hexagonal lattice for the $L_{\beta'}$ phase.

thins, such as egg lecithin (for a review, see Ref. 17). In addition, Ververgaert *et al.* (18) have demonstrated the appearance of rippled structures for dilute dispersions of DLL, DPL, and DSL. Although a distribution of ripple periodicities are observed for each lecithin, one value predominates and this value is in good agreement with the value obtained by x-ray diffraction. A systematic study of the effect of quenching temperature on DML and DPL indicates that the ripple appearance is observed only when the sample is quenched from a temperature intermediate between the pretransition and chain-melting transition (19).[3]

Now we consider the thermal behavior for this series of compounds. It is well documented that the chain-melting transition temperature of aqueous dispersions of the synthetic lecithins progressively increases with increasing hydrocarbon chain length. The pretransition temperature also increases with increasing chain length and appears to be converging with the chain-melting transition. Extrapolation of the two lines would predict convergence of the two transitions by $C_{22:0}$. A pretransition temperature has not been reported for DLL probably because of the low temperature at which both transitions exist, occurring near the ice water transition. The fact that DML, DPL, and DLL all exhibit the structure $P_{\beta'}$ at temperatures below the chain-melting transition suggests that a pretransition does exist for DLL and by extrapolation would occur at ~−10°C.

We have shown that for DML and DPL, the pretransition is no longer observed in the hydration range near 20% water. Similar observations have been made for DSL. Thus, the pretransition is dependent on the amount of water present for DML, DPL, and DSL (no data are available for DLL). The interaction of water with the polar head group of lecithin has been investigated using a variety of techniques including DSC (20), hydrodynamic measurements (21), water vapor absorption (22), and nuclear magnetic resonance (23). These results indicate that the hydration shell (*i.e.* highly structured or bound water) for lecithin is 11 molecules of water/lecithin molecule. This corresponds to 23% water by weight for DLL, 22% for DML, 21% for DPL, and 20% for DSL. These values are close to the hydration value where the pretransition is no longer observed experimentally. Thus, the appearance of the pretransition is correlated with the existence of a complete hydration shell for the lecithin molecule. The fact that the pretransition temperature does not occur at a temperature defined by the chain-melting transition (*i.e.* T_3 minus a constant for each lecithin) may indicate that the hydrocarbon chains play some role in the appearance of the pretransition (see below).

From thermodynamic considerations, maximum hydration or the swelling limit of the lecithin will occur when the chemical potential of the water located interstitially between the bilayers is equal to that of bulk water. For lecithin, the swelling varies with the phase existing at a given temperature. For $L_{\beta'}$ and $P_{\beta'}$, the swelling limit occurs at 29% water for DML and 25% for DPL. From these observations for $L_{\beta'}$ and $P_{\beta'}$, maximum hydration corresponds to ~15 water molecules/lecithin molecule. In the phase L_α, the swelling behavior is well documented for DML, DPL, and DSL, the swelling limit of the lecithin occurring at 40 weight % water. This corresponds to 23 molecules of H_2O/molecule of DLL; 25 molecules of H_2O/molecule of DML; 27 molecules of H_2O/molecule of DPL; and 29 molecules of H_2O/molecule of DSL.

From these considerations, we propose a generalized representation of the phase behavior of the synthetic lecithins. The experimentally determined phase boundaries for DML and DPL, and the proposed phase boundaries for DLL and DSL, are shown in Fig. 14. The phases defined by these phase boundaries are those shown in Fig. 13, *i.e.* $L_{\beta'}$, $P_{\beta'}$, and L_α. Below the chain-melting transition, we suggest that the phase behavior for the synthetic lecithins is identical with respect to hydration. The appearance of the pretransition is associated with the formation of a hydration shell for the lecithin molecule, 11 molecules of H_2O/molecule of lecithin. The phases $L_{\beta'}$ and $P_{\beta'}$ swell to a limiting value of 15 molecules of water/lecithin molecule. This is in contrast to the swelling behavior above the chain-melting transition where maximum swelling for the L_α phase increases with increasing chain length.

The proposed differences and similarities above and below the chain-melting transition may be determined by the lipid-water interface of the phospholipid. For example, it would be expected that the surface area (S_l) of each lecithin would be similar below the chain-melting transition ($L_{\beta'}$ and $P_{\beta'}$) and variable above the transition (L_α). Complete data on the temperature dependence of S_l are not available on all the synthetic lecithins. However, S_l has been calculated as a function of temperature for DML and DPL and is presented in Fig. 15. The calculated surface areas for these two lecithins are very similar below T_3 and differ above T_3. For example, at T_3 + 22°C, the surface area for DLL is 59.4 Å^2, 62.0 Å^2 for DML, and 69.5 Å^2 for DPL. Furthermore, there appears to be an increase in S_l with increasing chain length above T_3.

The forces between bilayers are now considered in order to understand these differences in the swelling behavior. It has been proposed that the increase or decrease in the bilayer separation due to the variation in the water layer thickness can be correlated with the predicted weakening or strengthening of the attractive van der Waals forces between bilayers (24). These authors (24) have correlated the computed van der Waals attraction with the variation in the water layer

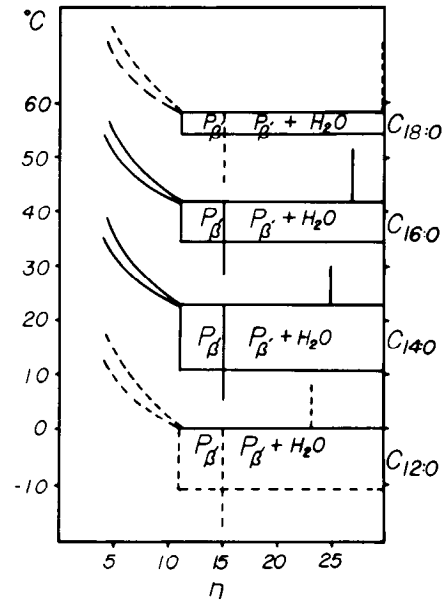

FIG. 14. Proposed generalized phase behavior of the synthetic lecithins, dilauroyl lecithin, dimyristoyl lecithin, dipalmitoyl lecithin, and distearoyl lecithin. *n*, the number of water molecules/lecithin molecule. The *solid lines* are phase boundaries based on experimental data; the *dashed lines* represent assumed phase boundaries (see text).

[3] A similar freeze fracture study (Gebhardt, C., Gruler, H., and Sackmann, E. (1977) *Z. Naturforsch* **32c**, 581–596) again shows the rippled structure only when DML is quenched from temperatures between the two transitions. However, using arguments derived from consideration of the types of lattice defects observed, these authors suggest that both nonsinusoidal ripples as well as variations in the tilt angle of the phospholipid across the ripple should be considered. To distinguish between these different versions of the structure of the rippled $P_{\beta'}$ phase requires higher resolution crystallographic studies.

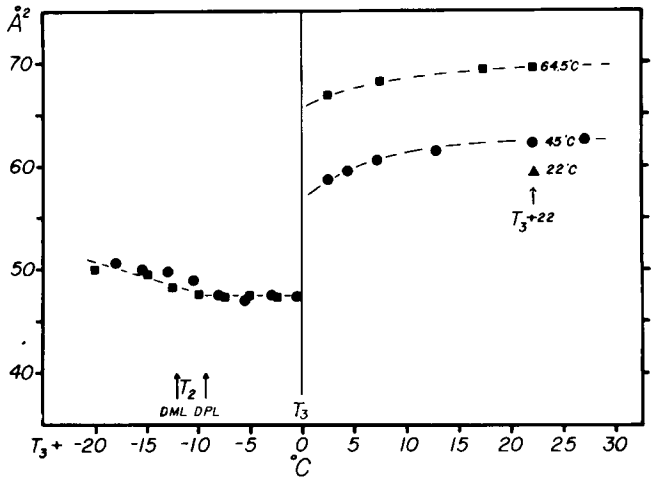

FIG. 15. Temperature dependence of the calculated surface area of DML (●) and DPL (■), both at maximum hydration. ▲, dilauroyl lecithin data from Ref. 13.

thickness between bilayers for egg lecithin. These results indicate that a decrease in the attractive energy between bilayers results in an increase in the water layer thickness. Below the chain-melting transition, the surface areas are very similar for DML and DPL, and may be the same for DLL and DSL. If so, the attractive forces would be distributed over the same area for each lecithin and the swelling behavior would be identical. Above the chain-melting transition, the surface area increases with increasing chain length. The attractive forces at each surface of two adjacent bilayers would then be dispersed over a larger area for each lecithin of increasing chain length. Thus, the net attractive forces between bilayers would decrease and an increase in the interstitial water between bilayers would result. This would lead to an increase in maximum swelling of the lecithin with increasing chain length above T_3.

Acknowledgments—We wish to thank Dr. D. M. Engelman (Yale University) for the use of the position-sensitive detector x-ray diffraction system. We wish to thank Ms. Sarah Brady for typing the manuscript.

REFERENCES

1. Danielli, J. F., and Davson, H. (1935) *J. Cell Comp. Physiol.* **5,** 495–508
2. Shipley, G. G. (1973) in *Biological Membranes* (Chapman, D., and Wallach, D. F. H., eds) Vol. 2, pp. 1–89, Academic Press, New York
3. Chapman, D. (1976) *Q. Rev. Biophys.* **8,** 185–235
4. Lee, A. G. (1975) *Prog. Biophys. Mol. Biol.* **29,** 3–56
5. Chapman, D., Williams, R. M., and Ladbrooke, B. D. (1967) *Chem. Phys. Lipids* **1,** 445–475
6. Tardieu, A., Luzzati, V., and Reman, F. C. (1973) *J. Mol. Biol.* **75,** 711–733
7. Cubero Robles, E., and Van Den Berg, D. (1969) *Biochim. Biophys. Acta* **187,** 520–526
8. Janiak, M. J., Small, D. M., and Shipley, G. G. (1976) *Biochemistry* **15,** 4575–4580
9. Franks, A. (1958) *Br. J. Appl. Phys.* **9,** 349–352
10. Elliot, A. J. (1965) *J. Sci. Instrum.* **42,** 312–316
11. Mabrey, S., and Sturtevant, J. M. (1976) *Proc. Natl. Acad. Sci. U. S. A.* **73,** 3862–3866
12. Laggner, P., and Stabinger, H. (1976) *J. Colloid Interface Sci.* **5,** 91–96
13. Tardieu, A. (1972) Ph.D. thesis, Universite de Paris-Sud.
14. Torbet, J., and Wilkins, M. H. F. (1977) *J. Theor. Biol.* **62,** 447–458
15. Ranck, J. L., Mateu, L., Sadler, D. M., Tardieu, A., Gulik-Krzywicki, T., and Luzzati, V. (1974) *J. Mol. Biol.* **85,** 249–277
16. Levine, Y. K. (1970) Ph.D. thesis, University of London
17. Gulik-Krzywicki, T. (1975) *Biochim. Biophys. Acta* **415,** 1–28
18. Ververgaert, P. H. J. Th., Verkleij, A. J., Elbers, P. F., and Van Deenen, L. L. M. (1973) *Biochim. Biophys. Acta* **311,** 320–329
19. Luna, E. J., and McConnell, H. M. (1977) *Biochim. Biophys. Acta* **466,** 381–392
20. Ladbrooke, B. D., and Chapman, D. (1969) *Chem. Phys. Lipids* **3,** 304–367
21. Hauser, H. (1975) in *Water—A Comprehensive Treatise* (Franks, F., ed) pp. 209–303, Plenum Press, New York
22. Elworthy, P. H. (1961) *J. Chem. Soc.* 5385–5389
23. Finer, E. G., and Darke, A. (1974) *Chem. Phys. Lipids* **12,** 1–16
24. Le Neveu, D. M., Rand, R. P., Gingell, D., and Parsegian, V. A. (1975) *Science* **191,** 399–400